Evaluation of ^{11}C-NR2B-SMe and Its Enantiomers as PET Radioligands for Imaging the NR2B Subunit Within the NMDA Receptor Complex in Rats

Lisheng Cai[1], Jeih-San Liow[1], Cheryl L. Morse[1], Sanjay Telu[1], Riley Davies[1], Michael P. Frankland[1], Sami S. Zoghbi[1], Ken Cheng[2], Matthew D. Hall[2], Robert B. Innis[1], and Victor W. Pike[1]

[1]*Molecular Imaging Branch, National Institute of Mental Health, National Institutes of Health, Bethesda, Maryland; and* [2]*NCATS Chemical Genomics Center, National Institutes of Health, Rockville, Maryland*

[*S-methyl*-^{11}C](±)-7-methoxy-3-(4-(4-(methylthio)phenyl)butyl)-2,3,4,5-tetrahydro-1*H*-benzo[*d*]azepin-1-ol (^{11}C-NR2B-SMe) and its enantiomers were synthesized as candidates for imaging the NR2B subunit within the *N*-methyl-D-aspartate receptor with PET. **Methods:** Brains were scanned with PET for 90 min after intravenous injection of one of the candidate radioligands into rats. To detect any NR2B-specific binding of radioligand in brain, various preblocking or displacing agents were evaluated for their impact on the PET brain imaging data. Radiometabolites from brain and other tissues were measured ex vivo and in vitro. **Results:** Each radioligand gave high early whole-brain uptake of radioactivity, followed by a brief fast decline and then a slow final decline. ^{11}C-(*S*)-NR2B-SMe was studied extensively. Ex vivo measurements showed that radioactivity in rat brain at 30 min after radioligand injection was virtually unchanged radioligand. Only less lipophilic radiometabolites appeared in plasma. High-affinity NR2B ligands, Ro-25-6981, ifenprodil, and CO101244, showed increasing preblocking of whole-brain radioactivity retention with increasing dose (0.01–3.00 mg/kg, intravenously). Five σ_1 antagonists (FTC146, BD1407, F3, F4, and NE100) and 4 σ_1 agonists ((+)-pentazocine, (±)-PPCC, PRE-084, and (+)-SKF10047) were ineffective preblocking agents, except FTC146 and F4 at a high dose. Two potent σ_1 receptor agonists, TC1 and SA4503, showed dose-dependent preblocking effects in the presence or absence of pharmacologic σ_1 receptor blockade with FTC146. **Conclusion:** ^{11}C-(*S*)-NR2B-SMe has adequate NR2B-specific PET signal in rat brain to warrant further evaluation in higher species. TC1 and SA4503 likely have off-target binding to NR2B in vivo.

Key Words: NR2B subunit; NMDA receptor; GluN2B; sigma 1; NR2B-SMe

J Nucl Med 2020; 61:1212–1220
DOI: 10.2967/jnumed.119.235143

N-methyl-D-aspartate (NMDA) receptors are ligand and voltage-gated ion channels that mediate influx of Ca^{2+}, Na^+, and K^+ into the synapse (*1*). These receptors are expressed throughout the central nervous system and play key physiologic roles in synaptic plasticity, learning, and memory. NMDA receptors are also implicated in the pathophysiology of several central nervous system disorders (*2–4*) and more recently have been identified as a target for the treatment of disease-associated genomic variation (*5*). NMDA receptors exist as diverse subtypes as a result of variation in the assembly of 7 subunits (NR1, NR2 subunits [NR2A−NR2D], and NR3 [A or B]) into tetrameric receptor complexes. Unique structural features of the NMDA receptor subtypes account for the tuning of their physiologic roles and their distinct pharmacologic properties. NMDA receptors, especially those enriched with NR2B subunits, endow the prefrontal cortex not only with important functionality but also with a major vulnerability to environmental insults and to risk factors for psychiatric disorders (*6*).

NMDA receptors have distinct binding sites for L-glutamate, glycine, D-serine, polyamines, Mg^{2+}, phencyclidine, and Zn^{2+}. Ligands for NMDA are of 4 types, namely glutamate binding site ligands, glycine binding site ligands, channel blockers, and *N*-terminal domain binding ligands. Some NMDA ligands have been developed into drugs, such as memantine for the treatment of Alzheimer disease (*7,8*). Attempts to produce radioligands for imaging NMDA receptors in living subjects with PET is an active area of research that has nonetheless met with only limited success (*9,10*).

NR2B is the most studied subunit within the NMDA receptor complex. This subunit is expressed throughout the central nervous system, with the highest concentration in the forebrain and the dorsal horn of the spinal cord (*11*). The NR2B subunit is a therapeutic target for schizophrenia, stroke, and neurodegenerative diseases, especially neuropathic pain. Therapeutics targeting NR2B rather than the NMDA channel may have fewer side effects. The quantification of NMDA NR2B subunit receptors in vivo with PET could help to elucidate the contribution of this receptor to neuropsychiatric disorders and also assist in drug development (*10*). A promising PET radioligand for NR2B, named ^{11}C-(*R*)-Me-NB1, has been reported very recently and shows modest displaceable signal for NR2B in rats in vivo (*12,13*).

Here, within a broader medicinal chemistry campaign to develop PET radioligands with high specific signal and low background noise, we discovered (±)-7-methoxy-3-(4-(4-(methylthio)phenyl) butyl)-2,3,4,5-tetrahydro-1*H*-benzo[*d*]azepin-1-ol (NR2B-SMe) (chemical structure is shown in Supplemental Fig. 1; supplemental materials are available at http://jnm.snmjournals.org). This compound shows high affinity for NR2B in the nanomolar range, moderate lipophilicity, and amenability to labeling with ^{11}C (half-life, 20.4 min). We therefore prepared ^{11}C-NR2B-SMe and its enantiomers from

Received Aug. 14, 2019; revision accepted Dec. 19, 2019.
For correspondence or reprints contact: Lisheng Cai, Molecular Imaging Branch, National Institute of Mental Health, National Institutes of Health, 10 Center Dr., Building 10, Room B3 C346, Bethesda, MD 20892.
E-mail: lishengcai@mail.nih.gov
Published online Jan. 10, 2020.

S-methyl propionyl precursors for evaluation as NR2B PET radioligands in rats.

MATERIALS AND METHODS

General Methods

Animal Experiment Ethics and Approval. All animal experiments were performed in accordance with the *Guide for the Care and Use of Laboratory Animals* (https://grants.nih.gov/grants/olaw/guide-for-the-care-and-use-of-laboratory-animals.pdf) and were approved by the National Institute of Mental Health Animal Care and Use Committee.

Statistics. Subsequent numeric data are expressed as mean ± SD for $n > 2$, or as mean and range for $n = 2$.

Absolute Configuration and In Vitro Properties. The absolute configurations of (–)-NR2B-SMe and (+)-NR2B-SMe were determined by vibrational circular dichroism.

Radiosynthesis

Preparation of ^{11}C-NR2B-SMe. (±)-methyl 3-((4-(4-(1-hydroxy-7-methoxy-1,2,4,5-tetrahydro-3*H*-benzo[*d*]azepin-3-yl)butyl)phenyl) thio)propanoate (NR2B-ester; 0.5 mg; 1.1 μmol) in dimethylformamide (0.40 mL) and *tetra-n*-butylammonium hydroxide in methanol (5 μL of 1 M stock solution in MeOH; 5 μmol) were loaded into a septum-sealed reaction vial (1-mL neck vial; Waters Corp.) of a Synthia apparatus (*14*). ^{11}C-iodomethane (>37 GBq) was then swept with a stream of helium (15 mL/min) into the vial from a Microlab module and left at room temperature for 5 min. ^{11}C-NR2B-SMe was separated out with high-performance liquid chromatography (HPLC) on a Luna C18 column (10 μm, 4.6 × 250 mm; Phenomenex) eluted at 6 mL/min for 20 min with trifluoroacetic acid (0.1% w/v) in MeCN water (35:65 v/v). Eluate was monitored for absorbance at 255 nm and radioactivity. The fraction containing ^{11}C-NR2B-SMe (retention time, 10.0 min) was collected in ascorbic acid solution (10 mg/mL; 0.1 mL) and then rotary-evaporated to dryness (80°C, water bath). The residue was dissolved in sterile saline for injection (4 mL) containing ethanol (1 mL) and aqueous $NaHCO_3$ solution (8.4% w/v; 40 μL). The solution (pH ~5.5) was sterile-filtered into a sterile and pyrogen-free dose vial that had been preloaded with sterile saline for injection (5 mL).

This product was analyzed with HPLC on an X-Bridge C18 column (10 μm, 4.6 × 250 mm; Waters Corp.) eluted for 15 min with trifluoroacetic acid (0.1% w/v) in MeCN water (40:60 v/v) at 1.5 mL/min. Eluate was monitored for absorbance at 255 nm and for radioactivity. The retention time of ^{11}C-NR2B-SMe was 9.5 min. The response of the analytic system had been calibrated for the mass of NR2B-SMe to allow molar activity to be calculated.

The identity of the radioligand was confirmed by its comobility in analytic HPLC with added reference compound and by liquid chromatography–mass spectrometry of residual carrier after decay of the formulated radioligand overnight. The formulated radioligand had greater than 98% radiochemical purity. The stability of formulated ^{11}C-NR2B-SMe was assessed with radio-HPLC at 1 and 2 h after radiosynthesis.

Radiometabolites of ^{11}C-NR2B-SMe in Rat Tissues Ex Vivo

Rats were anesthetized with 1.5% isoflurane in oxygen. Formulated ^{11}C-NR2B-SMe (200 μL; 37 MBq) was then injected intravenously through the penile vein of each rat. Other experimental parameters related to this study are listed in Supplemental Table 1. Thirty minutes after injection of ^{11}C-NR2B-SMe, a large anticoagulated (heparin) blood sample was drawn from each rat. The rats were then immediately sacrificed by decapitation, and their brains and myocardial tissues were excised.

For Brain and Myocardium. The radioactive tissue was weighed, placed in acetonitrile (1 mL), measured for radioactivity, and homogenized along with carrier NR2B-SMe (50 μg) using a handheld tissue Tearor (model 985-370; BioSpec Products Inc.). Water (500 μL) was then added, and the tissue was further homogenized before measurement of radioactivity. The homogenate was centrifuged at 10,000*g* for 1 min. The supernatant was then analyzed with general HPLC method A (NR2B-SMe; retention time, ~6.4 min). The precipitate was measured for radioactivity to determine the recovery of radioactivity in the supernatant that had been injected onto the HPLC column.

For Plasma. Plasma was separated from blood cells, and a sample (50 μL) was measured for radioactivity. An aliquot (450 μL) was placed in acetonitrile (720 μL) along with carrier NR2B-SMe (5 μg) and mixed well. Water (100 μL) was added, mixed well, measured for radioactivity, and centrifuged at 10,000*g* for 1 min. The supernatant was analyzed with radio-HPLC and the precipitate measured for radioactivity, as described for brain.

The stability of ^{11}C-NR2B-SMe in rat tissues ex vivo was determined by dividing the percentage of radioactivity present as radioligand in the tissue sample measured with HPLC by the fractional radiochemical purity of the radioligand (Table 1).

The SUV due to radioligand or radiometabolite only was calculated by multiplying the total SUV of the tissue by the fraction of the radioligand or radiometabolite measured with HPLC (Table 2).

TABLE 1
Ex Vivo and In Vitro Stabilities of ^{11}C-NR2B-SMe in Rat Tissues

Radioactive sample	Ex vivo stability (%)	In vitro stability (%)
Whole blood		89.8
Plasma	71.6	90.4
Brain	99.2	97.0
Myocardium	90.0	

Measurements were made at 30 min after intravenous injection of radioligand ex vivo and at 30 min after incubation of radioligand at 37°C in vitro. Stabilities are represented by ratios of percentage of parent radioligand in tissue to fractional radioligand purity at start of study. Formulated radioligand was initially 98.4% pure and found to be 99.2% intact 3 h later at end of other measurements.

PET Imaging in Rats

Selection of Agents for Preblocking and Displacement for PET Experiments in Rats. The aims of preblocking and displacement experiments were to assess radioligand target engagement and to determine radioligand selectivity in vivo. Many ligands do not show

TABLE 2
Concentrations of ^{11}C-NR2B-SMe in Rat Tissues and Tissue-to-Plasma Radioactivity Ratios Measured Ex Vivo at 30 Minutes After Intravenous Injection

Radioactive sample	SUV	Tissue-to-plasma ratio
Whole blood	0.047	1.6
Plasma	0.03	1.0
Brain	2.59	86.3
Myocardium	0.30	10.1

TABLE 3
Pharmacologic Parameters for ^{11}C-NB1 and ^{11}C-NR2B-SMe

Radioligand	NR2B K_i (nM)	σ_1 ligand binding inhibition at 10 μM (%)	σ_1 K_i (nM)	σ_2 ligand binding inhibition at 10 μM (%)	σ_2 K_i (nM)
^{11}C-NB1 (*12*)	9.8	89	182	88	554
^{11}C-NR2B-SMe	2.2	84		90	

selectivity for binding to NR2B over σ_1 receptors (*15–19*). In addition, σ_1 receptors exist in close proximity on cell membranes and may have direct interactions with NMDA receptors, modulating the behavior of NMDA receptor complexes (*20*). NR2B-SMe showed high binding affinity to the NR2B receptor but also showed weak binding affinity to σ_1 receptors in vitro (Table 3). To address NR2B-SMe selectivity in PET imaging, we chose various NR2B, σ_1, and σ_2 ligands for preblocking and displacement experiments in normal rats in vivo with PET. The studied NR2B ligands are summarized in Table 4, σ_1 antagonists and ligands of undetermined σ_1 intrinsic efficacy in Table 5, and putative σ_1 agonists in Table 6.

Estimation of ED_{50} Values In Vivo from Dose–Response Data. After administering ^{11}C-NR2B-SMe or one of its enantiomers to rats at baseline, the whole-brain radioactivity concentration (SUV) was seen to almost stabilize by 20 min (Fig. 1). The SUV unit normalizes radioactivity concentration for rat weight and injected dose. We used the SUVs of time–activity curves of the deployed radioligand between 20 and 90 min to calculate areas under the curve (AUCs). AUCs obtained from the same production of radioligand were scaled to the value (or mean value) for the baseline experiment to give relative values (dubbed relative AUC 20–90 min) (Fig. 1). These data were used to estimate the dose of blocking agent that was effective for a 50% reduction of the AUC 20–90 min at baseline, here termed ED_{50} and reported as moles of administered blocker per kilogram of body weight. Where data permitted, the dose–response curves were fitted with GraphPad Prism software (version 8.1.1) to estimate the ED_{50} values. A dummy value of 100 pmol per kilogram of body weight was used for zero concentration of the challenge agent in the construction of these dose–response curves.

RESULTS

NR2B-SMe and Its Chemical Properties

Absolute Configuration. (–)-NR2B-SMe and (+)-NR2B-SMe were found to have *R* and *S* absolute configuration, respectively, as determined by comparison of vibrational circular dichroism and infrared spectra measured with the calculated Boltzmann-averaged spectra of the calculated conformations (Supplemental Figs. 2 and 3; Supplemental Table 2), after separation of the racemic mixture by chiral HPLC columns (Supplemental Figs. 4 and 5).

Binding Affinities In Vitro and Other Physical Properties. The K_i value of NR2B-SMe in the in vitro assay in transiently transfected mouse fibroblast cells expressing NMDA was 2.2 nM (Table 3). The acid dissociation constant (p*K*a) was determined to be 5.04 (Supplemental Fig. 6), and the partition coefficient ($\log D_{7.4}$) was 3.41.

Pharmacologic Screen. NR2B-SMe was found to be selective for binding to the NR2B subunit because a 10 μM concentration only weakly inhibited the binding of reference radioligands to numerous binding sites and receptors. At a 10 μm concentration, inhibition was greater than 10% for only a few binding sites and receptors. These were the calcium channel (10.6%), hERG channels (66.3%), guinea pig σ_1 (83.7%), and PC12 cell σ_2 (90.0%).

*Experiments on HeLa Cells (*21*).* NR2B-SMe failed to compete with Cy3 dye for lysosome trapping in HeLa cells, in contrast with the positive control, loperamide (Supplemental Fig. 7).

Experiments with ^{11}C-NR2B-SMe in Rats and Human Tissues

Stability of ^{11}C-NR2B-SMe in Rat Whole Blood, Plasma, and Brain Ex Vivo and In Vitro. The radiochemical purity of ^{11}C-NR2B-SMe was 98.4% throughout the experiment (duration, ~3 h), after HPLC separation (Supplemental Fig. 8) and formulation (Supplemental Fig. 9).

At least 3 radiometabolites eluted before ^{11}C-NR2B-SMe in the reversed-phase HPLC analyses of rat plasma ex vivo (Supplemental Fig. 10A). These were very minor in brain and myocardium ex vivo (Supplemental Figs. 10B and 10C). Unchanged

TABLE 4
In Vitro and In Vivo Pharmacologic Parameters for NR2B Ligands

Ligand	Tissue NR2B K_i assay	Reference radioligand for NR2B K_i assay	K_i for NR2B (nM)	K_i for other targets (nM)	ED_{50} in vivo* (nmol/kg)
NR2B-SMe	Oocytes	^{3}H-ifenprodil	2.0		9.5
Ro-25-6981		^{3}H-MK801	9.0 (*37*)		29
CO101244	Oocytes	Electric current	43 (*38*)		74
Ifenprodil	Rat	^{3}H-ifenprodil	46.3 (*39*)	σ_1 = 11 (*39*) σ_2 = 1.1	211

*For preblocking of binding of ^{11}C-NR2B-SMe in rat whole brain measured in this study.

TABLE 5
In Vitro and In Vivo Pharmacologic Parameters for σ_1 Receptor Ligands (Not Identified as Agonists)

σ_1 ligand	Tissue for K_i assays	K_i for σ_1* (nM)	K_i for σ_2† (nM)	ED_{50} in vivo‡ (nmol/kg)
FTC146	Rat liver homogenate	0.0025 (*35,36*)	364	2571
BD1047	Guinea pig brain	0.9 (*40*)	47	>1,000
NE100	Guinea pig brain	1.03 (*41*)	211	>1,000
F3	Rat brain homogenate	0.79 (*42*)	277	138
F4	Rat brain homogenate	2.30 (*42*)	327	>1,000

*Reference radioligand ^{3}H-pentazocine, except ^{18}F-FTC146 for FTC146.
†Reference radioligand ^{3}H-DTG.
‡For preblocking of ^{11}C-(*S*)-NR2B-SMe rat whole-brain uptake measured in this study.

radioligand at 30 min after injection accounted for 71.6% of radioactivity in rat plasma, 99.2% in brain, and 90% in myocardial tissue (Table 1). Brain and myocardium showed high ratios of radioligand concentration (SUV) to that in plasma (Table 2). Ex vivo radioactivity in plasma distributed 51% to blood cells (*22*). The radiometabolites in vitro are the same as those observed ex vivo (Supplemental Fig. 11).

Plasma Free Fraction of ^{11}C-NR2B-SMe. The human plasma free fraction of ^{11}C-NR2B-SMe was 0.82% ± 0.01% (n = 3).

Evaluation of ^{11}C-NR2B-SMe and Its Enantiomers in Rats with PET

After intravenous injection of a bolus of racemic ^{11}C-NR2B-SMe into rat, there was a rapid and high uptake of radioactivity in brain followed by a quick decline to a moderately high stable level (Fig. 2A; Supplemental Fig. 12A). Relatively high uptakes were seen in thalamus, striatum, and cortex (Fig. 2A). When rats were intravenously administered NR2B-SMe or the NR2B ligand ifenprodil, at 3.0 mg/kg at 10 min before ^{11}C-NR2B-SMe, the peak whole-brain and brain regional radioactivity uptake declined to a common low level at 90 min, corresponding to about 10% of peak values in the baseline experiment (Fig. 2A). Accordingly, summed PET images before and after ifenprodil treatment were strikingly different (Fig. 2B). Administration of the NR2B ligand Ro-25-6981 at 10 min after radioligand resulted in a dose-dependently faster whole-brain radioactivity decline (Supplemental Fig. 12B).

The separate homochiral radioligands gave slightly different time–activity curves in whole brain (Fig. 3). The *R*-enantiomer (Fig. 3A) showed a somewhat faster radioactivity decline from peak value than the *S*-enantiomer (Fig. 3B). Intravenous injection of the NR2B ligand Ro-25-691 at 10 min before either homochiral radioligand lowered whole-brain retention of radioactivity. The effect was greater at the higher dose of 0.05 mg/kg than the lower dose of 0.01 mg/kg. As seen for the racemic radioligand, Ro-25-6981 administered at 10 min after the *R*-enantiomer resulted in a dose-dependently faster whole-brain radioactivity decline (Supplemental Fig. 12C).

The abilities of NR2B ligands to preblock whole-brain radioactivity uptake before intravenous injection of ^{11}C-(*S*)-NR2B-SMe into rats was studied in more detail. The time–activity curves for ^{11}C-NR2B-SMe and each enantiomer showed dose-dependent preblocking by NR2B-SMe itself (Figs. 1 and 3C) and by the NR2B ligands ifenprodil (Supplemental Fig. 13A) and CO101244 (Supplemental Fig. 13C). Sigmoidal dose–response curves (relative AUC 20–90 min vs. dose) for NR2B-SMe (Fig. 3C), ifenprodil (Supplemental Fig. 13B), and CO101244 (Supplemental Fig. 13D), as well as for the NR2B ligand Ro-25-6981 (Fig. 3C), were readily fitted to provide ED_{50} values (nmol/kg) (Table 4). These ED_{50} values were in rank order of their NR2B binding potencies ($1/K_i$) in vitro (Table 4).

σ_1 receptor antagonists, such as BD1047, NE100, and F4, showed minimal preblocking of radioactivity retention in whole rat brain before the administration of ^{11}C-(*S*)-NR2B-SMe (Supplemental

TABLE 6
In Vitro and In Vivo Pharmacologic Parameters for Putative σ_1 Receptor Agonists

Ligand	Tissue for K_i assays	K_i for σ_1* (nM)	K_i for σ_2† (nM)	ED_{50} in vivo‡ (nmol/kg)
TC1	Guinea pig brain	10 (*43*)	370	45
SA4503	Guinea pig membranes	17.4 (*44,45*)	1,784	29
	Rat brain membranes	4.6 (*36,39*)	63	
(+)-pentazocine	Guinea pig brain	13.7 (*44,46*)	2,875	>1,000
(±)-PPCC	Guinea pig brain	1.5 (*47*)	50.8	>1,000
PRE-084	Guinea pig brain	44 (*48,49*)		>1,000
(+)-SKF10047	Guinea pig brain	48 (*50*)	625	>1,000

*Reference radioligand ^{3}H-pentazocine, except ^{3}H-(+)-SKF-10047 for PRE-084.
†Reference radioligand ^{3}H-DTG.
‡For preblocking of ^{11}C-(*S*)-NR2B-SMe rat whole-brain uptake measured in this study.

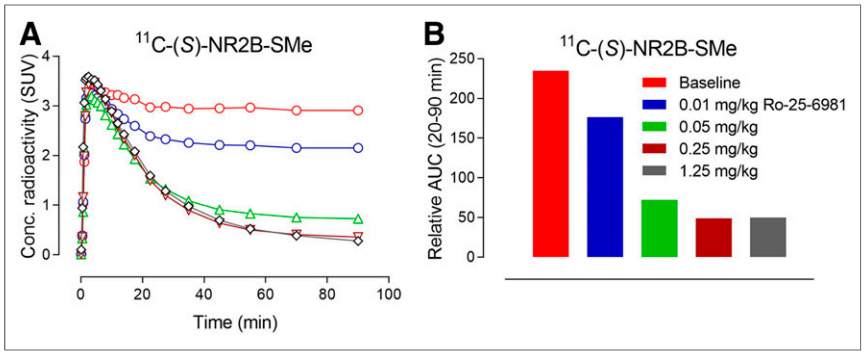

FIGURE 1. (A) Ro-25-6981 dose-dependently preblocks rat whole-brain radioactivity uptake from intravenous injection of ^{11}C-(*S*)-NR2B-SMe. (B) AUC between 20 and 90 min from A for ^{11}C-(*S*)-NR2B-SMe at different dose of preblocking agent Ro-25-6981, highly selective antagonist for NR2B receptor. Data are for $n = 1$.

Fig. 14). No meaningful sigmoidal dose–response curves could be fitted for these data, showing that the ED_{50} values for these ligands were much greater than 1,000 nmol/kg, in contrast to their affinities for σ_1 receptors in vitro, which are in the low nanomolar range (Table 5), or for the affinity of BD19147 at σ_2 receptors, which is quite low at 47 nM (Table 5). The very high affinity σ_1 receptor antagonist FTC146 caused preblocking only at a high dose of 1.25 mg/kg intravenously (Fig. 4A). The σ_1 ligand F3 also showed a dose-dependent preblocking effect (Supplemental Fig. 14). Dose–response curves could be fitted for FTC146 (Fig. 4B) and F3 (Supplemental Fig. 14) and allowed ED_{50} values to be estimated. These ED_{50} values were found to be extremely high relative to their K_i values at σ_1 receptors in vitro (Table 5).

σ_1 receptor agonists, such as (+)-pentazocine, (±)-PPCC, PRE-084, and (+)-SKF10047 (Supplemental Fig. 15), showed very weak preblocking effects on radioactivity retention in whole rat brain before administration of ^{11}C-(*S*)-NR2B-SMe. These data could not be fitted to sigmoidal dose–response curves, and ED_{50} estimates were therefore extremely high (>1,000 nmol/kg) (Table 6). Exceptionally, the σ_1 agonists TC1 (Fig. 5A) and SA4503 (Fig. 6A) showed dose-dependent preblocking effects that could be fitted to sigmoidal dose–response curves (Figs. 5C and 6C, respectively). The ED_{50} values for TC1 and SA4503 were estimated to be quite low at 45 and 29 nmol/kg, respectively (Table 6). However, the preblocking effects of these 2 σ_1 agonists were unaltered when the potent σ_1 receptor antagonist, FTC146, was used to pharmacologically block σ_1 receptors (Figs. 5 and 6). The respective dose–response curves (Figs. 5B, 6B, 5C, and 6C) were congruent with those obtained in the absence of σ_1 receptor blocking with FTC146.

DISCUSSION

We were able to resolve the enantiomers of NRB2B-SMe by chiral HPLC. Knowledge of the absolute configuration of NR2B-SMe could be valuable in future NR2B ligand design. We were able to assign the absolute configurations of NR2B-SMe enantiomers successfully with infrared and vibrational circular dichroism.

^{11}C-NR2B-SMe and its enantiomers were readily prepared for intravenous injection into rats by treating NR2B ester with ^{11}C-methyl iodide under basic conditions. The radiolabeling process is likely a reverse Michael addition of α,β-unsaturated acrylic acid or ester (Supplemental Fig. 1) (*23*). ^{11}C-NR2B-SMe decomposed when concentrated immediately after HPLC isolation, but the decomposition was minimal after ascorbic acid was added during the removal of mobile phase. A constant radiochemical purity of greater than 98% was then achieved.

Initial PET experiments on rats used racemic ^{11}C-NR2B-SMe. These experiments showed that ^{11}C-NR2B-SMe readily entered brain, peaking at approximately 3 SUVs in whole brain at about 2.5 min (Fig. 2A). Peak radioactivity was followed by a slow decline in radioactivity. Radioactivity retention in brain regions such as thalamus, cortex, and cerebellum could be preblocked with NR2B-SMe itself and by the NR2B ligand ifenprodil (Fig. 2A). Thalamus and cortex are generally considered to be NR2B-rich regions. However, appreciable specific binding in cerebellum would not have been expected on the basis of previous in vitro autoradiography of postmortem rat brain with NR2-specific antibody (*24*). Our finding of specific binding in cerebellum that can be blocked by ifenprodil is consistent with findings of Krämer et al. (*12*), who observed high specific binding of their putative NR2B radioligand, ^{11}C-Me-NB1, to rat cerebellum with both in vitro autoradiography and ex vivo biodistribution measurements. Yet, deeper investigations are needed to verify that specific binding in cerebellum is to NR2B. The radioactivity in brain could be partially displaced by the NR2B radioligand Ro-25-6981, suggesting reversibility of radioligand binding to NR2B (Supplemental Fig. 12).

At 30 min after intravenous administration, unchanged radioligand represented virtually all rat brain radioactivity (>99%), a finding that was highly favorable to pursuing further radioligand characterization. Parent ^{11}C-NR2B-SMe represented close to 70% of radioactivity in plasma at 30 min

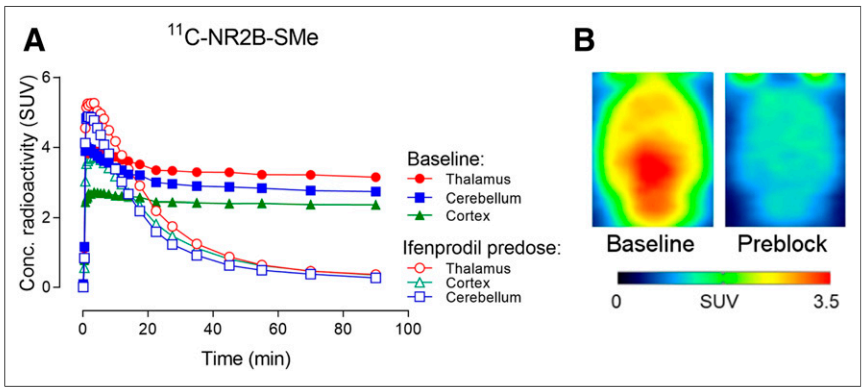

FIGURE 2. PET imaging of rat brain with racemic ^{11}C-NR2B-SMe. (A) PET time–activity curves for selected brain regions in rat after intravenous injection of ^{11}C-NR2B-SMe showing that brain radioactivity accumulation is blocked by preadministration of ifenprodil at 3.0 mg/kg (intravenous). (B) Summed transaxial PET images (60–90 min) from ^{11}C-NR2B-SMe at baseline and after preblocking with NR2B ligand ifenprodil. Data are for $n = 1$.

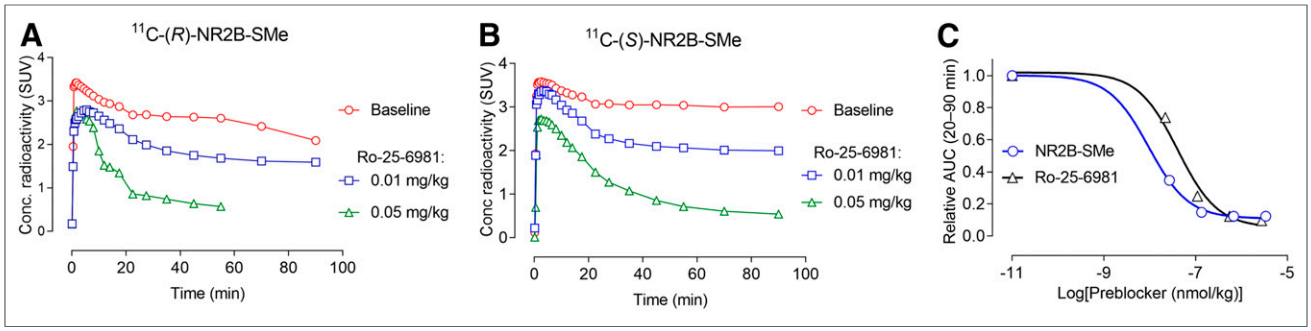

FIGURE 3. (A and B) Blocking of whole-brain radioactivity uptake in rat by dosing with NR2B ligand Ro-25-6981 before intravenous injection of ^{11}C-(*R*)-NR2B-SMe (A) and ^{11}C-(*S*)-NR2B-SMe (B). (C) Fitted dose–response curves derived from B for NR2B-SMe and from A in Figure 1 for NR2B ligand Ro-25-6981. Data are for $n = 1$.

after injection of ^{11}C-NR2B-SMe, showing that peripheral metabolism in vivo was relatively slow (Table 1). ^{11}C-NR2B-SMe showed a high accumulation in NR2B-rich heart (*25*), as well as in brain relative to blood (Table 2). ^{11}C-NR2B-SMe also showed high metabolic stability in rat whole blood, plasma, and brain in vitro (Table 1).

Because ^{11}C-NR2B-SMe was strongly retained in rat brain at baseline, we investigated whether trapping in lysosomes might be responsible. Lysosomes are membrane-bound organelles found in nearly all animal cells (*26*). With a pH ranging from 4.5 to 5.0, the interior of the lysosomes is acidic whereas cytosol is slightly basic (pH 7.2). Protonated weak bases may accumulate within lysosomes, in some cases reaching 100- to 1,000-fold higher concentrations than the extracellular concentration, a phenomenon known as lysosomotropism (*27*) or proton pump effect (*28*). The accumulation of compounds in lysosomes may be estimated from compound pK_a (*29*). NR2B-SMe is monobasic. The optimal pK_a range for lysosomal trapping of a monobasic compound is between 6 and 10. Therefore, we measured the p*K*a of ^{11}C-NR2B-SMe. We also investigated the uptake of NR2B-SMe into HeLa cell lysosomes in vitro.

The apparent pK_a of ^{11}C-NR2B-SMe was found to be 5.04 ± 0.01 ($n = 3$) (Supplemental Fig. 6). Therefore, ^{11}C-NR2B-SMe will be protonated to only a very low extent (0.63%) at the physiologic pH of cytosol (pH 7.2) but will be protonated to a greater extent (76%–50%) in lysosomes (pH 4.5–5.0). The pK_a of ^{11}C-NR2B-SMe, however, suggested a low risk for lysosomal trapping.

Conclusive evidence against lysosomal trapping of ^{11}C-NR2B-SMe came from experiments on HeLa cells, in which NR2B-SMe competes with the cyanine dye Cy3 for cell uptake. The greenish yellow fluorescence of the dye did not change on addition of NR2B-SMe, just as with addition of dimethylsulfoxide only, whereas the dye was excluded from the cells with loperamide (50 μM), a known ligand for lysosome trapping (*30*).

The lipophilicity of a PET radioligand, as indexed by log*D* at pH 7.4, is a key property that influences many aspects of PET radioligand behavior in vivo (*31*), including brain entry, metabolism, and protein binding. We found the log$D_{7.4}$ of ^{11}C-NR2B-SMe to be 3.41, which is close to that predicted by computation (2.98) and in the range for many successful PET radioligands for central nervous system targets.

The stability of ^{11}C-NR2B-SMe in human brain homogenate and human plasma and the plasma free fraction in vitro were of interest with respect to possible eventual radioligand application in human subjects. ^{11}C-NR2B-SMe was virtually unchanged when exposed to these tissues for 30 min at room temperature in vitro, suggesting that radiometabolites would not be generated in human brain in vivo.

The plasma free fraction of a PET radioligand can be an important parameter for the use of a PET radioligand for quantifying a protein target in human subjects. The human plasma free fraction for ^{11}C-NR2B-SMe in human plasma was relatively low, but measurable with good precision (0.82% ± 0.01%, $n = 3$).

Generally, PET radioligands should not be used as racemates because their enantiomers may show differences in binding affinities for their targets and possibly other differences in, for example, kinetics and metabolism. Given the encouraging PET results and encouraging in vitro measures with racemic ^{11}C-NR2B-SMe, we proceeded to evaluate the enantiomers of ^{11}C-NR2B-SMe. Each homochiral radioligand showed brain uptake similar to that of the racemic radioligand in rats. The *S*-enantiomer showed a slower decline in whole-brain radioactivity concentration from peak value than did the *R*-enantiomer. The NR2B ligand Ro-25-6981 was effective in blocking the brain retention of radioactivity from both enantiomers, suggesting they both show specific binding to NR2B (Fig. 3). As also seen for the racemic radioligand, radioactivity in brain from the *R*-enantiomer could be displaced with Ro-25-6981 in a dose-dependent manner, thereby confirming the reversibility of specific binding (Supplemental Fig. 12). Because ^{11}C-(*S*)-NR2B-SMe

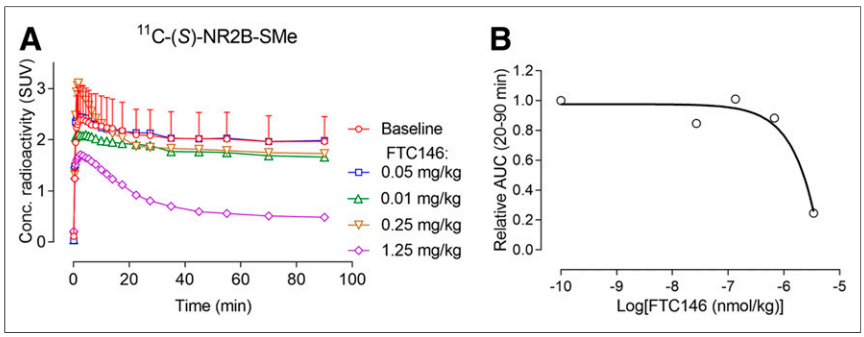

FIGURE 4. (A) Low to moderate preadministered intravenous doses of highly potent σ_1 receptor antagonist FTC146 do not reduce whole-brain radioactivity in rats after intravenous injection of ^{11}C-(*S*)-NR2B-SMe. (B) Fitted dose–response curve for FTC146 derived from data in A. Baseline data are mean for $n = 2$. Error bar represents range. Other data are for $n = 1$.

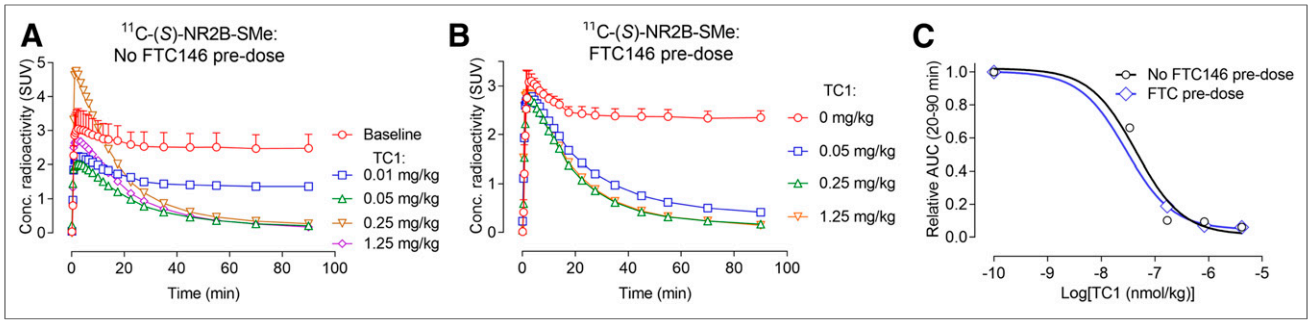

FIGURE 5. (A) Intravenous preadministration of TC1 dose-dependently reduces rat whole-brain radioactivity uptake from intravenous injection of ^{11}C-(*S*)-NR2B-SMe. (B) Intravenous preadministration of TC1 in rats that have been simultaneously pretreated with FTC146 (0.05 mg/kg, intravenously) at 10 min before ^{11}C-(*S*)-NR2B-SMe dose-dependently reduces whole-brain radioactivity uptake. (C) Fitted dose–response curves from A and B data. Curves in A and B are highly congruent, as are curves in C, showing no effect of σ_1 receptor blockade by FTC146. Baseline data are mean for $n = 2$. Error bar represents range. Other data are for $n = 1$.

showed the stronger retention in rat brain, subsequent experiments were performed with this radioligand. They were primarily directed at exploring the specificity of the PET signal.

In total, we used 3 NR2B ligands (Ro-25-6981, CO-101244, and ifenprodil) and NR2B-SMe itself as preblocking agents at various doses for PET experiments on ^{11}C-(*S*)-NR2B-SMe in rats. Each ligand gave data that could be fitted to a dose–response curve for the estimation of ED_{50} values in vivo. The ED_{50} values were in rank order of the K_i values in vitro (Table 6). These results are therefore consistent with ^{11}C-NR2B-SMe selectively occupying the NR2B binding site in rat brain in vivo.

σ_1 receptors are transmembrane proteins expressed in many different tissues. They are particularly concentrated in certain regions of the central nervous system (*32*) and may function as a chaperone to NMDA receptors (*33,34*). Five antagonists of the σ_1 receptor (FTC146, BD1047, NE100, F3, and F4) had very limited preblocking effects on the PET radioligand ^{11}C-NR2B-SMe (Fig. 4; Supplemental Fig. 14; Table 5), further suggesting that ^{11}C-NR2B-SMe does not occupy σ_1 receptors. Four of 6 tested σ_1 receptor agonists had only weak preblocking effects (i.e., high ED_{50} values) (Supplemental Fig. 14; Table 6). However, 2 putative selective σ_1 agonists, TC1 and SA4503, had strong effects on the brain uptake of ^{11}C-NR2B-SMe (Figs. 5 and 6; Table 6). We considered that these 2 ligands might have off-target binding to NR2B receptors. Therefore, we designed preblocking PET experiments with TC1 or SA4503 and ^{11}C-(*S*)-NR2B-SMe in which σ_1 receptors would be pharmacologically blocked with the high-affinity antagonist FTC146 (K_D = 2.5 pM). For these experiments, we selected an FTC146 dose of 0.05 mg/kg (intravenous), which we estimated would achieve an exceptionally high peak brain concentration of 134 nM, which should assuredly occupy all σ_1 receptors, even if the brain free fraction was exceptionally low. This estimate was based on published data (^{18}F-FTC146 peak brain uptake, ~1 SUV in mice) (*35,36*). The effects of TC1 and SA4503 on brain uptake of ^{11}C-(*S*)-NR2B-SMe were the same as in the absence of FTC146 (Figs. 5 and 6, respectively). Therefore, preblocking of σ_1 receptors did not prevent interactions of TC1 and SA4503 with the NR2B receptor. This strongly suggests that these σ_1 agonists have some affinity for NR2B receptors. Also, these data further suggest that ^{11}C-(*S*)-NR2B-SMe does not have appreciable off-target binding to σ_1 receptors in rat brain in vivo.

CONCLUSION

Racemic ^{11}C-NR2B-SMe binds selectively and with high affinity to the NR2B subunit. Absolute configurations were successfully assigned to the enantiomers of NR2B-SMe. ^{11}C-NR2B-SMe and its enantiomers were readily prepared as prospective radioligands for PET imaging of NR2B subunits within NMDA receptors. In normal rats, these radioligands show high initial brain radioactivity uptake, followed by slow washout. The radioactivity

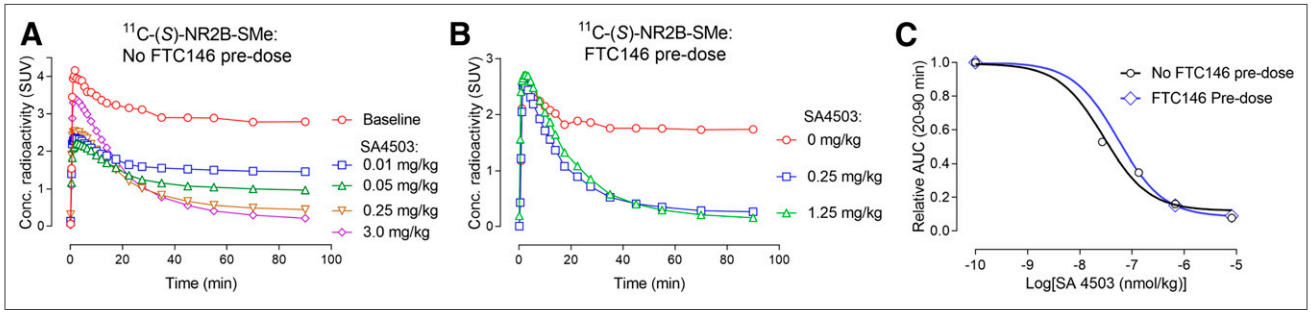

FIGURE 6. (A) Preadministered intravenous doses of SA4503 reduced whole-brain radioactivity uptake in rats from intravenous injection of ^{11}C-(*S*)-NR2B-SMe. (B) Simultaneous intravenous preadministration of SA4503 and FTC146 (0.05 mg/kg, intravenously) at 10 min before ^{11}C-(*S*)-NR2B-SMe dose-dependently reduced whole-brain radioactivity uptake. (C) Fitted dose–response curves derived from A and B data. Curves in A and B are highly congruent, as are curves in C, showing no effect of σ_1 receptor blockade by FTC146. Data are for $n = 1$.

in brain is predominantly unchanged radioligand and is not trapped in lysosomes. ^{11}C-(*S*)-NR2B-SMe shows a slower decline in brain concentration than its antipode. Brain uptake of this radioligand is reversible and can be preblocked up to 90% with a variety of NR2B ligands in a dose-dependent way. Brain uptake of ^{11}C-NR2B-SMe cannot be preblocked by σ_1 receptor antagonists, consistent with the radioligand occupying the NR2B binding site, not the σ_1 receptor. However, brain uptake of ^{11}C-(*S*)-NR2B-SMe can be preblocked by 2 of 6 σ_1 receptor agonists, consistent with a direct interaction of the 2 agonists with NR2B. Altogether, this study suggests that ^{11}C-(*S*)-NR2B-SMe has adequate NR2B-specific PET signal in rat brain to warrant yet deeper investigation of its specific binding across brain regions, including cerebellum, and further evaluation as a radioligand in higher species.

DISCLOSURE

This study was funded by the Intramural Research Program of the National Institute of Mental Health, National Institutes of Health: projects ZIAMH002795 and ZIAMH002793. No other potential conflict of interest relevant to this article was reported.

ACKNOWLEDGMENTS

We thank Dr. Mary Herman (CDBD, National Institute of Mental Health) for postmortem human brain tissues. We also thank the NIH PET Department for ^{11}C production, PMOD Technologies for providing the image analysis software, and PDSP for performing assays: the PDSP is directed by Bryan L. Roth, PhD, with project officer Jamie Driscoll (National Institute of Mental Health) at the University of North Carolina Chapel Hill (contract NO1MH32004).

KEY POINTS

QUESTION: Can we image the brain NR2B receptor using PET?

PERTINENT FINDINGS: PET imaging using normal rats has shown that ^{11}C-NR2B-SMe in both racemic and chiral forms has specific signal that can be preblocked and displaced using ligands specifically targeting NR2B receptors but not using ligands specifically targeting σ_1 receptors.

IMPLICATIONS FOR PATIENT CARE: ^{11}C-NR2B-SMe has potential as a PET radioligand to measure the distribution of NR2B receptors in human brain.

REFERENCES

1. Hansen KB, Yi F, Perszyk RE, et al. Structure, function, and allosteric modulation of NMDA receptors. *J Gen Physiol.* 2018;150:1081–1105.
2. Li XH, Miao HH, Zhuo M. NMDA receptor dependent long-term potentiation in chronic pain. *Neurochem Res.* 2019;44:531–538.
3. Tanqueiro SR, Ramalho RM, Rodrigues TM, Lopes LV, Sebastiao AM, Diogenes MJ. Inhibition of NMDA receptors prevents the loss of BDNF function induced by amyloid beta. *Front Pharmacol.* 2018;9:237.
4. Theibert HPM, Carroll BT. NMDA antagonists in the treatment of catatonia: a review of case studies from the last 10 years. *Gen Hosp Psychiatry.* 2018;51:132–133.
5. Ueda K, Serajee F, Huq AM. Clinical benefit of NMDA receptor antagonists in a patient with ATP1A2 gene mutation. *Pediatrics.* 2018;141(suppl):S390–S394.
6. Monaco SA, Gulchina Y, Gao WJ. NR2B subunit in the prefrontal cortex: a double-edged sword for working memory function and psychiatric disorders. *Neurosci Biobehav Rev.* 2015;56:127–138.
7. Song X, Jensen MO, Jogini V, et al. Mechanism of NMDA receptor channel block by MK-801 and memantine. *Nature.* 2018;556:515–519.
8. Zambrano P, Suwalsky M, Jemiola-Rzeminska M, Strzalka K. Studies on the interaction of NMDA receptor antagonist memantine with cell membranes: a mini-review. *Chem Biol Interact.* 2018;283:47–50.
9. Fu H, Chen Z, Josephson L, Li Z, Liang SH. Positron emission tomography (PET) ligand development for ionotropic glutamate receptors: challenges and opportunities for radiotracer targeting N-methyl-D-aspartate (NMDA), alpha-amino-3-hydroxy-5-methyl-4-isoxazolepropionic acid (AMPA) and kainate receptors. *J Med Chem.* 2019;62:403–419.
10. Kassenbrock A, Vasdev N, Liang SH. Selected PET radioligands for ion channel linked neuroreceptor imaging: focus on GABA, NMDA and nACh receptors. *Curr Top Med Chem.* 2016;16:1830–1842.
11. Zhuo M. Ionotropic glutamate receptors contribute to pain transmission and chronic pain. *Neuropharmacology.* 2017;112:228–234.
12. Krämer SD, Betzel T, Mu L, et al. Evaluation of ^{11}C-Me-NB1 as a potential PET radioligand for measuring GluN2B-containing NMDA receptors, drug occupancy, and receptor cross talk. *J Nucl Med.* 2018;59:698–703.
13. Haider A, Herde AM, Kramer SD, et al. Preclinical evaluation of benzazepine-based PET radioligands (R)- and (S)- ^{11}C-Me-NB1 reveals distinct enantiomeric binding patterns and a tightrope walk between GluN2B- and sigma1-receptor-targeted PET imaging. *J Nucl Med.* 2019;60:1167–1173.
14. Lu S, Giamis AM, Pike VW. Synthesis of ^{18}F-fallypride in a micro-reactor: rapid optimization and multiple-production in small doses for micro-PET studies. *Curr Radiopharm.* 2009;2:nihpa81093.
15. Avenet P, Leonardon J, Besnard F, et al. Antagonist properties of the stereoisomers of ifenprodil at NR1A/NR2A and NR1A/NR2B subtypes of the NMDA receptor expressed in Xenopus oocytes. *Eur J Pharmacol.* 1996;296:209–213.
16. Hashimoto K, London ED. Interactions of erythro-ifenprodil, threo-ifenprodil, erythro-iodoifenprodil, and eliprodil with subtypes of sigma receptors. *Eur J Pharmacol.* 1995;273:307–310.
17. Lengyel C, Dezsi L, Biliczki P, et al. Effect of a neuroprotective drug, eliprodil on cardiac repolarisation: importance of the decreased repolarisation reserve in the development of proarrhythmic risk. *Br J Pharmacol.* 2004;143:152–158.
18. Whittemore ER, Ilyin VI, Woodward RM. Antagonism of N-methyl-D-aspartate receptors by sigma site ligands: potency, subtype-selectivity and mechanisms of inhibition. *J Pharmacol Exp Ther.* 1997;282:326–338.
19. Bath CP, Farrell LN, Gilmore J, et al. The effects of ifenprodil and eliprodil on voltage-dependent Ca^{2+} channels and in gerbil global cerebral ischaemia. *Eur J Pharmacol.* 1996;299:103–112.
20. Pabba M, Sibille E. Sigma-1 and N-methyl-d-aspartate receptors: a partnership with beneficial outcomes. *Mol Neuropsychiatry.* 2015;1:47–51.
21. Kazmi F, Hensley T, Pope C, et al. Lysosomal sequestration (trapping) of lipophilic amine (cationic amphiphilic) drugs in immortalized human hepatocytes (Fa2N-4 cells). *Drug Metab Dispos.* 2013;41:897–905.
22. Makhro A, Wang J, Vogel J, et al. Functional NMDA receptors in rat erythrocytes. *Am J Physiol Cell Physiol.* 2010;298:C1315–C1325.
23. Cai L, Liow JS, Zoghbi SS, et al. Synthesis and evaluation of N-methyl and S-methyl ^{11}C-labeled 6-methylthio-2-(4′-N,N-dimethylamino)phenylimidazo[1,2-a]pyridines as radioligands for imaging beta-amyloid plaques in Alzheimer's disease. *J Med Chem.* 2008;51:148–158.
24. Wang YH, Bosy TZ, Yasuda RP, et al. Characterization of NMDA receptor subunit-specific antibodies: distribution of NR2A and NR2B receptor subunits in rat brain and ontogenic profile in the cerebellum. *J Neurochem.* 1995;65:176–183.
25. Tejero-Taldo MI, Chmielinska JJ, Gonzalez G, Mak TI, Weglicki WB. *N*-methyl-D-aspartate receptor blockade inhibits cardiac inflammation in the Mg^{2+}-deficient rat. *J Pharmacol Exp Ther.* 2004;311:8–13.
26. Kuehnel W. *Color Atlas of Cytology, Histology, and Microscopic Anatomy.* 4th ed. New York, NY: Thieme; 2003.
27. de Duve C, de Barsy T, Poole B, Trouet A, Tulkens P, Van Hoof F. Commentary: lysosomotropic agents. *Biochem Pharmacol.* 1974;23:2495–2531.
28. Traganos F, Darzynkiewicz Z. Lysosomal proton pump activity: supravital cell staining with acridine orange differentiates leukocyte subpopulations. *Methods Cell Biol.* 1994;41:185–194.
29. Trapp S, Rosania GR, Horobin RW, Kornhuber J. Quantitative modeling of selective lysosomal targeting for drug design. *Eur Biophys J.* 2008;37:1317–1328.
30. Kannan P, Brimacombe KR, Kreisl WC, et al. Lysosomal trapping of a radiolabeled substrate of P-glycoprotein as a mechanism for signal amplification in PET. *Proc Natl Acad Sci USA.* 2011;108:2593–2598.
31. Pike VW. Considerations in the development of reversibly binding PET radioligands for brain imaging. *Curr Med Chem.* 2016;23:1818–1869.
32. Weissman AD, Su TP, Hedreen JC, London ED. Sigma receptors in post-mortem human brains. *J Pharmacol Exp Ther.* 1988;247:29–33.

33. Chu UB, Ruoho AE. Biochemical pharmacology of the sigma-1 receptor. *Mol Pharmacol.* 2016;89:142–153.
34. Lee CH, Lu W, Michel JC, et al. NMDA receptor structures reveal subunit arrangement and pore architecture. *Nature.* 2014;511:191–197.
35. James ML, Shen B, Zavaleta CL, et al. New positron emission tomography (PET) radioligand for imaging sigma-1 receptors in living subjects. *J Med Chem.* 2012;55:8272–8282.
36. Shen B, James ML, Andrews L, et al. Further validation to support clinical translation of ^{18}F-FTC-146 for imaging sigma-1 receptors. *EJNMMI Res.* 2015; 5:49.
37. Fischer G, Mutel V, Trube G, et al. Ro 25-6981, a highly potent and selective blocker of N-methyl-D-aspartate receptors containing the NR2B subunit: characterization in vitro. *J Pharmacol Exp Ther.* 1997;283:1285–1292.
38. Zhou ZL, Cai SX, Whittemore ER, et al. 4-hydroxy-1-[2-(4-hydroxyphenoxy) ethyl]-4-(4-methylbenzyl)piperidine: a novel, potent, and selective NR1/2B NMDA receptor antagonist. *J Med Chem.* 1999;42:2993–3000.
39. Lever JR, Gustafson JL, Xu R, Allmon RL, Lever SZ. Sigma1 and sigma2 receptor binding affinity and selectivity of SA4503 and fluoroethyl SA4503. *Synapse.* 2006;59:350–358.
40. McCracken KA, Bowen WD, de Costa BR, Matsumoto RR. Two novel σ receptor ligands, BD1047 and LR172, attenuate cocaine-induced toxicity and locomotor activity. *Eur J Pharmacol.* 1999;370:225–232.
41. Berardi F, Ferorelli S, Colabufo NA, Leopoldo M, Perrone R, Tortorella V. A multireceptorial binding reinvestigation on an extended class of sigma ligands: N-[omega-(indan-1-yl and tetralin-1-yl)alkyl] derivatives of 3,3-dimethylpiperidine reveal high affinities towards sigma1 and EBP sites. *Bioorg Med Chem.* 2001;9:1325–1335.
42. Li Y, Wang X, Zhang J, et al. Synthesis and evaluation of novel ^{18}F-labeled spirocyclic piperidine derivatives as sigma1 receptor ligands for positron emission tomography imaging. *J Med Chem.* 2013;56:3478–3491.
43. Liu X, Banister SD, Christie MJ, et al. Trishomocubanes: novel sigma ligands modulate cocaine-induced behavioural effects. *Eur J Pharmacol.* 2007;555:37–42.
44. Matsuno K, Nakazawa M, Okamoto K, Kawashima Y, Mita S. Binding properties of SA4503, a novel and selective sigma 1 receptor agonist. *Eur J Pharmacol.* 1996;306:271–279.
45. Kawamura K, Ishiwata K, Tajima H, et al. In vivo evaluation of ^{11}C-SA4503 as a PET ligand for mapping CNS sigma(1) receptors. *Nucl Med Biol.* 2000;27:255–261.
46. Cagnotto A, Bastone A, Mennini T. ^{3}H-(+)-pentazocine binding to rat brain sigma 1 receptors. *Eur J Pharmacol.* 1994;266:131–138.
47. Prezzavento O, Campisi A, Ronsisvalle S, et al. Novel sigma receptor ligands: synthesis and biological profile. *J Med Chem.* 2007;50:951–961.
48. Maurice T, Su TP, Parish DW, Nabeshima T, Privat A. PRE-084, a sigma selective PCP derivative, attenuates MK-801-induced impairment of learning in mice. *Pharmacol Biochem Behav.* 1994;49:859–869.
49. Su TP, Wu XZ, Cone EJ, et al. Sigma compounds derived from phencyclidine: identification of PRE-084, a new, selective sigma ligand. *J Pharmacol Exp Ther.* 1991;259:543–550.
50. Walker JM, Bowen WD, Walker FO, Matsumoto RR, De Costa B, Rice KC. Sigma receptors: biology and function. *Pharmacol Rev.* 1990;42:355–402.

Erratum

In the article "Patient Travel Concerns After Treatment with ^{177}Lu-DOTATATE," by Kendi et al. (*J Nucl Med.* 2020;61:496–497), the following sentence mistakenly provides an incorrect time frame, and reference 2 is unnecessarily cited. The original sentence reads "It is important to counsel patients in detail about the possibility of radiation detection when traveling in the first 6 wk after each therapy cycle (*2*)." The amended sentence should read "*It is important to counsel patients in detail about the possibility of radiation detection when traveling after each therapy cycle.*" The authors regret the error.